journal of the mechanical behavior of biomedical materials 104 (2020) 103641

Contents lists available at ScienceDirect

Journal of the Mechanical Behavior of Biomedical Materials

journal homepage: http://www.elsevier.com/locate/jmbbm

In vitro comparison of 3D printed polylactic acid/hydroxyapatite and polylactic acid/bioglass composite scaffolds: Insights into materials for bone regeneration

Milda Alksne [a,*], Migle Kalvaityte [a], Egidijus Simoliunas [a], Ieva Rinkunaite [a], Ieva Gendviliene [b], Janis Locs [c], Vygandas Rutkunas [b], Virginija Bukelskiene [a]

[a] Institute of Biochemistry, Life Sciences Center, Vilnius University, Sauletekio Ave. 7, LT-10257, Vilnius, Lithuania
[b] Institute of Odontology, Faculty of Medicine, Vilnius University, Zalgirio Str. 115, LT-08217, Vilnius, Lithuania
[c] Rudolfs Cimdins Riga Biomaterials Innovations and Development Centre of RTU, Institute of General Chemical Engineering, Faculty of Materials Science and Applied Chemistry, Riga Technical University, Pulka 3, Riga, LV-1007, Latvia

ARTICLE INFO

Keywords:
Bone regeneration
3D printing
Polylactic acid
Hydroxyapatite
Bioglass

ABSTRACT

3D printing of polylactic acid (PLA) and hydroxyapatite (HA) or bioglass (BG) bioceramics composites is the most promising technique for artificial bone construction. However, HA and BG have different chemical composition as well as different bone regeneration inducing mechanisms. Thus, it is important to compare differentiation processes induced by 3D printed PLA + HA and PLA + BG scaffolds in order to evaluate the strongest osteoconductive and osteoinductive properties possessing bioceramics. In this study, we analysed porous PLA + HA (10%) and PLA + BG (10%) composites' effect on rat's dental pulp stem cells fate *in vitro*. Obtained results indicated, that PLA + BG scaffolds lead to weaker cell adhesion and proliferation than PLA + HA. Nevertheless, osteoinductive and other biofriendly properties were more pronounced by PLA + BG composites. Overall, the results showed a strong advantage of bioceramic BG against HA, thus, 3D printed PLA + BG composite scaffolds could be a perspective component for patient-specific, cheaper and faster artificial bone tissue production.

1. Introduction

Every year millions of people are affected by the loss of bone tissue due to trauma, inflammation or tumours. Until now, cases with critical size bone defects are treated by bone grafting techniques (De Witte et al., 2018).

There are three major bone graft categories that are commonly used in bone grafting surgical procedures: autografts, allografts, and xenografts (Chen et al., 2018). Bone grafting is considered as a "gold standard" in bone defects treatment (Chen et al., 2018), however, they still have some limitations - additional harvesting procedure, donor site morbidity, graft availability, immunological rejection, etc.(Roseti et al., 2017). Thus, scientists all around the world seek to create functional biocompatible, osteoconductive, and even osteoinductive artificial scaffolds for bone tissue regeneration.

Bone defects are patient specific, thus artificial bone grafts should be able to adapt their structure to fully substitute damaged area. However, scaffold inner structure also plays a crucial role in bone regeneration process. For complete bone integration into the tissue, constructed bone graft should have interconnected pores to allow patient cell immigration (Karageorgiou and Kaplan, 2005). It is widely accepted that the best osteoinduction is achieved with 100–500 μm interconnected pore scaffolds (Hannink and Arts, 2011; Karageorgiou and Kaplan, 2005; Sabree et al., 2015). Currently, porous scaffolds have been prepared by a number of methodologies and technologies, such as fused filament fabrication (FFF) (Alksne et al., 2019; Gregor et al., 2017; Malinauskas et al., 2014), stereolithography (Sabree et al., 2015), porogen leaching (Mao et al., 2018; Wang et al., 2010), freeze-drying (Xu et al., 2011), gas forming (Chen et al., 2012), foam replication (Li et al., 2015) and phase separation (Conoscenti et al., 2017; Zhao et al., 2012), however, only 3D printing technology allows complete and accurate control of inner and outer structure of the scaffolds (Lam et al., 2002). Moreover, this technology can be used to implement various imaging techniques, such as computed tomography and magnetic resonance to create patient bone defect-specific 3D tissue or scaffold model. Additionally, 3D printing is becoming more and more accessible to a wider range of people, thus

* Corresponding author. Vilnius University, Life Sciences Center, Institute of Biochemistry, Sauletekio Ave. 7, LT-10223, Vilnius, Lithuania.
E-mail address: milda.peciukaityte@gmail.com (M. Alksne).

https://doi.org/10.1016/j.jmbbm.2020.103641
Received 30 October 2019; Received in revised form 13 December 2019; Accepted 14 January 2020
Available online 20 January 2020

instruments and manufacturing process expenditures are continue to decrease (Burgio et al., 2018; Kuss et al., 2018).

A wide range of polymers is used in 3D printing industry, and some of them are compatible with bioprinting applications. There are many medical grade, US Food and Drug Administration and European Medicines Agency approved, polymers which can be used for bone tissue engineering, e.g., polylactic acid (PLA), polyglycolic acid, polycaprolactone (PCL), polyvinyl alcohol, polyethylene glycol etc. (Alconcel et al., 2011; Chong et al., 2013; Dorati et al., 2017). Among these polymers in the studies of osteogenesis, the most commonly used are PCL and PLA polyesters (Huang et al., 2018; Jing et al., 2017; Kim et al., 2017; Narayanan et al., 2016). The PCL polyester advantages are good biocompatibility, relatively slow degradation rate and less acidic breakdown products (Lowry et al., 1997; Williams et al., 2005). Despite these properties, PCL should be preferable for soft tissue engineering because it is a ductile polymer, which has low elastic modulus and high elongation at break (Pei et al., 2017; Scaffaro et al., 2016). Meanwhile, PLA is a semi-crystalline polymer with relative high elastic modulus and low elongation at break, mechanical properties which make it a perfect candidate for bone tissue engineering (Scaffaro et al., 2016). Moreover, PLA is also a biodegradable and bioactive polyester, which can be produced even from renewable sources such as starch and sugars (Lopes et al., 2012). Despite all these benefits of PLA, it has an unpreferably long biodegradation time, and its biodegradation products decrease pH in surrounding tissues, which can induce inflammation and autoimmune response. Yet, these disadvantages can be overcome by combining PLA with other materials, such as bioceramics (Böstman and Pihlajamäki, 2000).

One of the first studied bioceramic was hydroxyapatite (HA) (Deng et al., 2001; Kasuga et al., 2000; Marra et al., 1999). HA is used in bone tissue engineering research since it is very similar to a natural bone apatite (Baino et al., 2015). HA is the most stable ceramic with low solubility in physiological environment which is determined by temperature, pH, body fluids, etc (Jeong et al., 2019). In the organism, HA surface can act as a nucleating site for bone minerals, thus it displays good osteoconductive properties and promotes cell osteogenesis (induces formation of mineralised matrix, activates the expression of genes and proteins related to bone tissue formation) (Jeong et al., 2019; Zhang et al., 2016). In addition, HA does not cause inflammatory reactions when applied clinically, thus in medical applications its powders are used as a bone filler or it is powder coated on metal bone prostheses (Baino et al., 2015). Despite its positive properties, HA is brittle, has low mechanical stability and slow biodegradation/bioresorption, which makes it an unattractive structural material (Huang et al., 2018; Kim et al., 2006). Nevertheless, these HA disadvantages can be overcome by creating composite PLA + HA material.

Another promising ceramic is bioglass (BG). It is also used as bone defect filler. After implantation, BG strongly bonds to bone tissue and triggers its regeneration as well as new blood vessel formation (Baino et al., 2015). These BG properties are determined by its surface modifications which occur due to time-dependent BG degradation in the tissue. Repeatedly, after its implantation, BG surface forms an active layer of HA (Sanz-Herrera and Boccaccini, 2011) that provides an interface where host tissue could easily interact with BG. While this bioceramic is degrading over time, it releases soluble silica, calcium, sodium and phosphate ions which stimulate osteogenesis and angiogenesis (Baino et al., 2015; Cao and Hench, 1996; Jones et al., 2010; Qi et al., 2018). However, as in the case with HA, it is not easily shaped, although in combination with PLA it has great potential to be used for bone tissue engineering applications (Turnbull et al., 2018).

As mentioned before, HA or BG and PLA composites are showing great promise for use in bone tissue engineering. By combining these bioceramics with PLA polymer they can negate some of eachother's disadvantages. For example, the created composite will biodegrade faster in tissue compared to pure materials. HA and BG are alkaline materials, which neutralize PLA acidity resulting from its degradation (Zhang et al., 2016). Moreover, hydrophilicity of the bioceramics enable easier permeability of water into the polymer matrix, thus boosting PLA hydrolytic degradation by increasing the surface area where PLA and body fluids interact (Barbeck et al., 2017; Delabarde et al., 2011; Luo et al., 2019; Wang et al., 2016). Furthermore, studies show that PLA and HA or BG composites enhance stem cell osteogenesis and angiogenesis processes *in vitro* as well as bone regeneration *in vivo*, compared to pure PLA, HA and BG materials. These composites are also compatible with 3D printing applications (Barbeck et al., 2017; Chen et al., 2019; Kasuga et al., 2000; Zhang et al., 2017, 2016). Thus both PLA and HA or BG composites demonstrate high potential for use in bone tissue engineering, however, to the authors' knowledge, there are no studies which would compare 3D printed PLA and HA or BG composite scaffolds.

Adult mesenchymal stem cells (MSC) are commonly used as a tool for the assessment of scaffolds osteoinductivity, osteoconductivity and biofriendly properties *in vitro* (Jiang et al., 2013; Ko et al., 2013; Lin et al., 2009; Polini et al., 2011). Dental pulp stem cells (DPSC) are a perfect adult mesenchymal stem cell source that can be used for cell-scaffold interaction studies, as well as for personalised artificial bone construct production. These cells possess high proliferative, self-renewal, and multipotency capabilities (Alksne et al., 2019; Gronthos et al., 2002; Khanna-Jain et al., 2012; Potdar and Jethmalani, 2015; Tatullo et al., 2015; Verma et al., 2014). Importantly, DPSCs tend to spontaneously differentiate into osteogenic lineage (Monterubbianesi et al., 2019; Noda et al., 2019). All these properties make DPSCs a better choice than the most commonly used bone marrow stem cells (BMSC) in this kind of study. (Berebichez-Fridman and Montero-Olvera, 2018; Jiang et al., 2013; Polini et al., 2011).

We have previously demonstrated that low-cost 3D printed PLA macro (i.e. larger than cell diameter) structures without additional surface modifications could promote spontaneous stem cell osteogenic differentiation (Alksne et al., 2019). In this study, we tried to improve the osteoinductivity of these scaffolds and attenuate negative effects of PLA degradation by creating composite PLA + HA (10%) and PLA + BG (10%) filaments, which were then used for scaffold production. We aimed to evaluate the bioactive properties of the 3D printed PLA + HA and PLA + BG composite scaffolds and to compare their impact on rat DPSC osteogenesis *in vitro*. Both HA and BG bioceramics have shown great promise for use in bone tissue engineering, thus, it is very important to identify the differences between these two 3D printed composites to yield and substantiate the best polymer and ceramic composition for low cost, easily produced and high quality artificial bone graft construction.

2. Materials and methods

2.1. Materials for composite filament preparation

Raw materials used in this study for composite filament preparation were PLA (racemic polymer composed of D and L isoforms) beads (STP chem. solutions co., Ltd., Thailand) – particle size 100–800 μm, molecular weight 42 700 (g/mol); HA powder (Riga Technical University, Latvia) - particle size 50 μm; and BG 45S5 (XL Sci-Tech, Inc., USA) - particle size 38–75 μm.

2.2. Composite filament preparation

Composite materials were prepared by thoroughly mixing the PLA and HA or PLA and BG powders at mass ratio of 9:1; in the case of pure PLA filament, only PLA pellets were used. Before extrusion, the mixture was stored in a sealed bag with silica gel pellets to absorb all the moisture from the material, as otherwise, the extrusion process was hard to control due to bubble formation in the filament. A desktop extruder (Filabot Original, Filabot HQ) equipped with a 1.75 mm nozzle was used to fabricate the filament. The extruder was pre-heated to 145 °C. A self-made spooler with adjustable spooling speed was used to wind the

filament onto the reel. During the extrusion process, the temperature of the extruder was manually adjusted in the range of 140–145 °C when needed. The diameter of the prepared composite filament varied from 1.28 to 1.6 mm.

2.3. Scaffold production

Scaffolds were fabricated using an FDM 3D printer 2 (Pharaoh XD 20, Mass Portal). The printing head was computer-controlled in three axes of delta mode (x, y, z with a xyz speed of 35 mm/s). The nozzle diameter was 400 μm. The printing parameters were set as described in a previous study (Alksne et al., 2019). Scaffolds were designed with a pore size of 450 μm and a total porosity of 48%. The scaffold geometry was a 3D macro-structured woodpile with threads rotated at an angle of 60° in respect to the ones of the previous layer. Each scaffold layer consists of two 400 μm width and 200 μm height threads moulded together, which formed a 400 μm height layer. All scaffolds had eight layers (Fig. 1A). The dimensions of 3D printed scaffolds were 3 cm × 3 cm x 1.6 mm. For *in vitro* studies, scaffolds were cut into 1 cm × 1 cm x 1.6 mm pieces.

2.4. SEM imaging

A scanning electron microscope (Hitachi TM-1000) was used to analyse the surface and morphology of the scaffolds. The sides of the prepared scaffolds were prepared by cutting specimens with laser light filament fabrication technology, 10 mm from the sides. Scaffolds were scanned edgewise (15 images in total for each group). Thread height, width and distance between threads were measured using ImageJ (1.8.0_112).

2.5. Water absorption of scaffolds

For the evaluation of water absorption tested scaffolds (1 cm × 1 cm x 1.6 mm) were weighted, then immersed into the water for 24 h. After the predetermined time, specimens were removed from the water, drained and weighted again. The water absorption ratio of the samples was determined by the equation: water absorption (%) = $(W_t - W_0)/(W_0) \times 100$, where W_0 is the primary weight of samples and W_t is the weight of samples after 24 h incubation in the water.

2.6. Protein adsorption of scaffolds

To evaluate protein adsorption on to the scaffolds, the Bradford assay was performed (Myung et al., 2014). Briefly, the samples (1 cm × 1 cm x 1.6 mm) were immersed into fetal bovine serum (FBS; Gibco) for 24 h. After the predetermined time, scaffolds were removed from FBS, washed twice with PBS to remove leftover FBS. Afterwards, scaffolds were soaked in Bradford reagent (Thermo Scientific) and the total adsorbed amount of proteins was evaluated using microplate reader Varioskan Flash (Thermo Scientific), measuring absorbtion at 595 nm. For background measurements, the scaffolds immersed in PBS for 24 h were used.

2.7. Cell culture

Rat DPSCs were used for this study. The use of rat DPSCs and their extraction from teeth procedure was approved by license of Animal research ethics committee (Lithuania) No. G2-40, 2016-03-18. Cell isolation and characterization protocols are described in (Alksne et al., 2019). Isolated DPSCs were maintained in growth medium (GM): Iscove's Modified Dulbecco's Medium (IMDM; Gibco) supplemented with 10% FBS and penicillin - 100 U/mL, streptomycin 100 mg/mL antibiotics solution (Gibco) at 37 °C in a humidified atmosphere containing 5% CO_2. The cells used in the experiments were up to 20 passages.

2.8. Cellular adhesion efficiency

To evaluate cell adhesion efficiency, DPSCs were grown (5×10^4 cell/cm^2) on tested samples for 0.5, 2 and 24 h. After predetermined time points, cultured cells were fixed with 4% paraformaldehyde (Carl Roth, GmbH) in phosphate-buffered saline (PBS; Gibco) for 15 min at room temperature (RT) with 25 rpm shaking. Next, samples were washed trice with 0.2% Triton X-100 (AppliChem GmbH) in PBS for 5 min at RT and stained with 5 U/mL rhodamine-phalloidin (Merck Millipore) and 12.5 μg/mL 4′,6-Diamidino-2-Phenylindole (DAPI; Life Technologies, Inc.) solution in PBS for 1 h at RT in the dark. Samples were washed trice with PBS for 5 min at RT; stained F-actin filaments were visualized by fluorescence inverted microscope (Olympus IX51). Quantitative differences in cells' adhesion efficiency were calculated by measuring the DPSCs surface area on different scaffolds at predetermined time points using an image processing program ImageJ (1.8.0_112).

2.9. Cellular adhesion strength

Cell adhesion strength on tested scaffolds was qualitatively and quantitatively evaluated by visualising focal adhesions (FA) within the cells 24 h after seeding (5×10^4 cell/cm^2) on different scaffolds. Cultured cells were fixed with 4% paraformaldehyde prepared in PBS for 15 min at RT with 25 rpm shaking. Then samples were washed trice with 0.2% Triton X-100 in PBS for 5 min at RT and blocked for 1 h with 3% Bovine serum albumin (BSA; AppliChem GmbH) and 10% FBS prepared in PBS. After blocking procedure, specimens were incubated with primary mouse anti-vinculin antibody (1:50; Merck Millipore) for 1 h at RT with 25 rpm shaking. Then, samples were washed trice with 0.05% Tween-20 (Sigma-Aldrich Co.) in PBS for 5 min and incubated with secondary goat anti-mouse antibodies conjugated with Alexa Flour 488 (Invitrogen) and 12.5 μg/mL DAPI solution in PBS for 1 h at RT in the dark with 25 rpm agitation. The samples were washed trice with PBS for 5 min at RT and visualized by fluorescence inverted microscope (Olympus IX51). Quantitative differences in cell adhesion strength were determined by counting FA within the cells using image processing program ImageJ (1.8.0_112).

2.10. Cell migration

For evaluation of cells migration on tested scaffolds, DPSCs (5×10^4 cell/cm^2) were seeded in tissue culture plate wells. After 24 h, tested scaffolds were placed on the formed cell monolayer and incubated for 72 h. Then, specimens were transferred to the new plate wells and washed with PBS. The numbers of cells which have migrated on each scaffold were determined by Crystal Violet assay. Briefly, samples were stained with 0.1% crystal violet (Sigma-Aldrich Co.) in 20% Ethanol (EtOH; Vilniaus degtinė) for 30 min with 25 rpm shaking. Then, the specimens were washed trice with deionized water and the crystal violet was dissolved in the elution buffer (0.1% acetic acid (Sigma-Aldrich Co.) in 50% EtOH) and incubated for 10 min. Dissolved crystal violet absorbance was measured using a microplate spectrophotometer Varioskan Flash (Thermo Scientific) at 590 nm. As a background value, scaffolds without cells were used.

2.11. Cell proliferation

In proliferation experiments, DPSCs (3×10^4 cell/cm^2) were grown on tested scaffolds for 24, 48, 72, 96 and 120 h. After predetermined time points, cell counts on different specimens were determined using DAPI assay as described in (Alksne et al., 2019). Cells were lysed by freezing in −20 °C and cellular DNA was dissolved in 0.04% sodium dodecyl sulfate (SDS)/saline-sodium citrate solution (Sigma-Aldrich Co.). DNA concentrations in the samples were evaluated with DAPI dye, by measuring its fluorescence (Ex. 360 nm, Em. 460 nm). As a

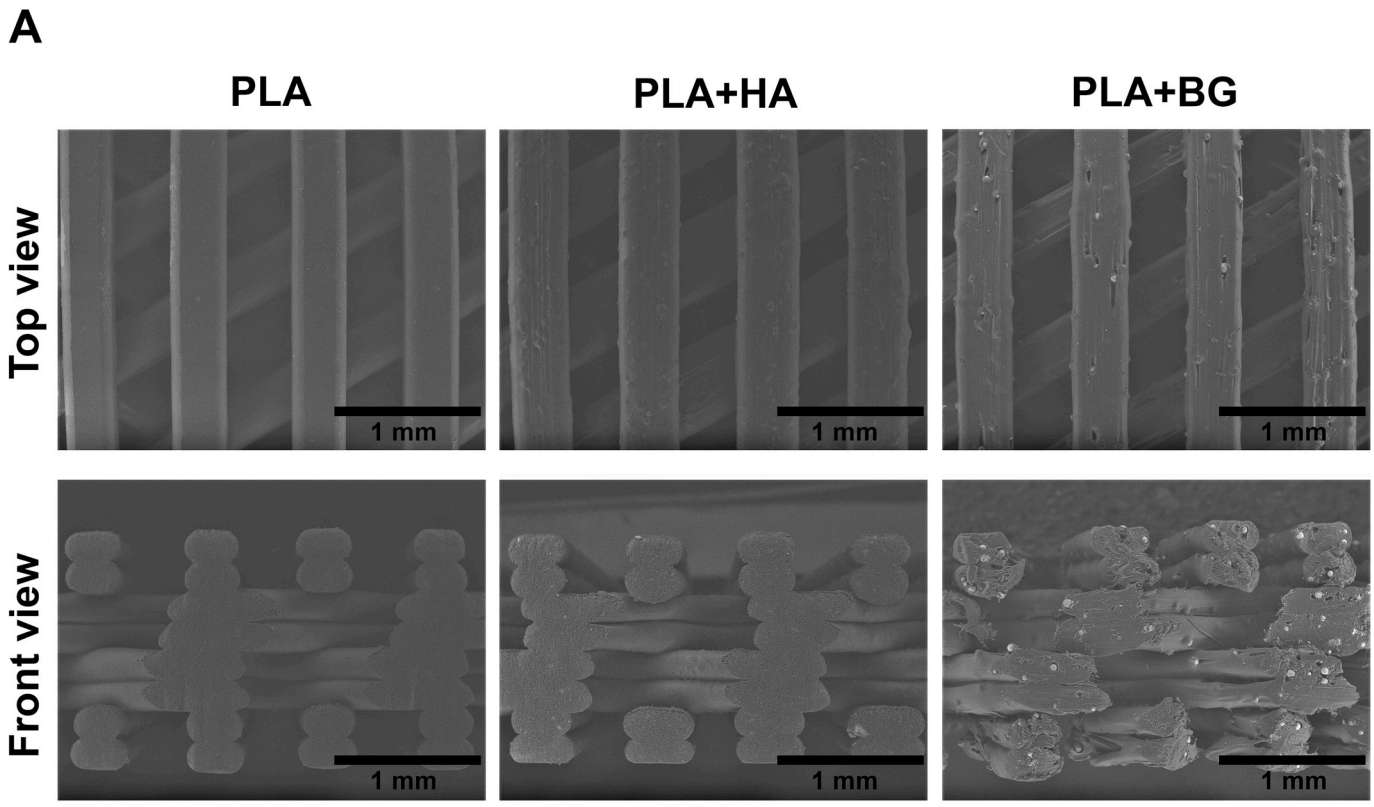

B

	PLA	PLA + HA	PLA + BG
Pore size, mm	414.4 ± 23.4	412.3 ± 10.9	396.9 ± 25.5
Thread height, mm	219.4 ± 8.4	224.0 ± 9.5	218.0 ± 10.2
Thread width,mm	387.9 ± 10.8	407.6 ± 17.9	384.4 ± 13.0

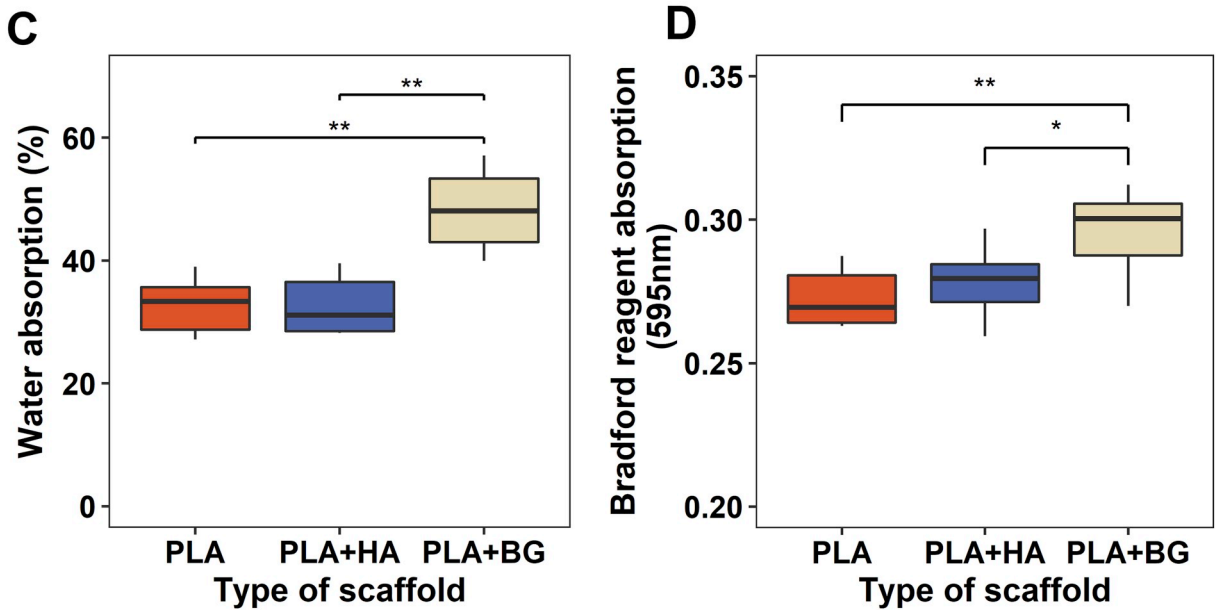

Fig. 1. The properties of 3D printed composite scaffolds: A – SEM images of the scaffolds' top and front views; B –dimensions of scaffold threads and pores; C – hydrophobicity of the composites; D – protein adsorption on 3D scaffolds quantification by Bradford assay. Statistically significant data are indicated as ** ($p < 0.01$).

background value, scaffolds without cells were used. Results were standardized according to the cell numbers determined on the appropriate composites after 24 h of incubation.

2.12. Osteogenic differentiation efficiency assessment

For DPSCs spontaneous osteogenic differentiation evaluation, cells (seeded cell number noted in Table 1) were grown on different composite scaffolds for 1, 7 and 10 days. Specimens were maintained in basic GM at 37 °C in a humidified atmosphere containing 5% CO_2; half of GM was changed every second/third day.

2.12.1. Alkaline phosphatase activity

Alkaline phosphatase (ALP) activity was detected using Phosphatase Substrate Kit (Thermo Scientific). All procedures were performed as described in (Alksne et al., 2019). Cells grown on tested scaffolds were immersed in 1 mg/mL p-Nitrophenyl phosphate (PNPP) solution and after 1 h of incubation 2 M NaOH (Merck Millipore) was added to stop ALP reaction. The reaction product was measured with spectrophotometer Varioskan Flash (Thermo Scientific) at 405 nm. As a background value, scaffolds without cells were attributed. Obtained data were normalised according to cell numbers which were determined on each type of scaffold after 1, 7 and 10 days.

2.12.2. Collagen amount

The amount of collagen in the extracellular matrix (ECM) was determined using Sirius red assay. At 1, 7 and 10 days' time points, GM was discarded; specimens were washed twice with PBS. Then, 1 mg/mL Direct red 80 (Sigma-Aldrich Co.) dissolved in 1.3% picric acid (Sigma-Aldrich Co.) was added to each sample and incubated for 1 h at RT with 25 rpm shaking. Afterwards, Sirius Red solution was removed; the samples were washed with 0.01 N HCl (Sigma-Aldrich Co.) in PBS and centrifuged at 100 g for 30 s (centrifuge HERMLE Labortechnik GmbH). Sirius Red residues on the scaffolds were dissolved in 0.1 N NaOH (Sigma-Aldrich Co.) in PBS, by incubating for 30 min at RT with 25 rpm shaking. The absorbance was measured using a microplate spectrophotometer Varioskan Flash (Thermo Scientific) at 550 nm. As a background value, scaffolds without cells were used.

2.12.3. Osteogenesis-related gene expression

Osteogenesis-related proteins Runx2, Osteopontin (OPN), and Osteocalcin (OCN) coding genes expression was evaluated using qPCR assay. RNA extraction, cDNA synthesis, and qPCR assays were performed as described in (Alksne et al., 2019). Cells grown on scaffolds were lysed with TRIzol Reagent (Ambion, Life Technologies, Inc.) and RNA extraction was performed using according to its manual in combination with PureLink RNA Mini Kit (Invitrogen, CA, USA). For cDNA synthesis 391 ng of RNA was used and the reaction was performed by RevertAid First Strand cDNA Synthesis Kit (Thermo Scientific). Quantification was implemented by qPCR with Maxima SYBR Green/ROX qPCR Master Mix (2X) (Thermo Scientific). The comparative $2^{-\Delta\Delta Ct}$ method was used to quantify genes' expression levels (Livak and Schmittgen, 2001). Primers sequences used for qPCR analysis are shown in Table 2. Data was normalised according to glyceraldehyde-3-phosphate dehydrogenase (GAPDH) gene expression and gene expression was further standardized to levels measured for undifferentiated cells, seeded on tissue culture plate surface at initial time point.

Table 1
The amount of cells which were seeded on the scaffolds for analysis of osteogenic differentiation at the corresponding time points.

Time points	Cell count
Day 1	1×10^5 cell/cm^2
Day 7	3×10^3 cell/cm^2
Day 10	3×10^3 cell/cm^2

Table 2
Sequences of analysed gene primer pairs used for qPCR.

Gene	Primer
OPN	FW: 5'-CCAGCCAAGGACCAACTACA-3' RV: 5'-TGGCTACAGCATCTGAGTGTTT-3'
OCN	FW: 5'-TGCATTCTGCCTCTCTGACC-3' RV: 5'-CTGGGGCTCCAAGTCCATTG-3'
Runx2	FW: 5'-TGAGATTTGTAGGCCGGAGC-3' RV: 5'-GCTTCTGTCTGTGCCTTCTTG-3'
GAPDH	FW: 5'-AGTGCCAGCCTCGTCTCATA-3' RV: 5'-ATGAAGGGGTCGTTGATGGC-3'

2.12.4. Mineralisation assay

Calcium deposits within DPSCs produced ECM were quantitatively evaluated using Alizarin red S (ARS) staining. All the procedures were performed as described in (Alksne et al., 2019). Cells grown on the scaffolds were fixed with 4% paraformaldehyde and stained with 2% ARS (Sigma-Aldrich Co.) solution. ARS residues were dissolved in 5% perchloric acid (AppliChem, GmbH) and measured with spectrophotometer Varioskan Flash (Thermo Scientific) at 490 nm. As a background value, scaffolds without cells were used.

2.13. Statistical analysis

R program package (RStudio v1.1.442) was used to perform statistical analysis. Data were reported as median ± IQR (of at least 3 independent experiments, $N \geq 3$ samples per group). The number of FA within cells are presented with distribution density function. Data normality was evaluated using Shapiro-Wilk test (when $n \geq 5$). Significant differences of not normally distributed results, between three and more groups were evaluated by Kruskal–Wallis one-way analysis of variance test; *post hoc* Tukey test was used to highlight differences in data. Normally distributed data (also, when $n < 5$) with three and more groups was evaluated using a one-way analysis of variance (ANOVA) and subsequently analysed with the *post hoc* Tukey test. p-values < 0.05 were considered to be statistically significant.

3. Results

3.1. Physical characteristics of the scaffolds

Composite scaffold materials were produced by mixing pure PLA beads with HA or 45S5 BG particles (mass ratio 9:1). The composite filaments were fabricated using filament extruder. We used the maximal amount of the bioceramics, which still had mechanical properties compatible with FFF manufacturing method. Obtained filaments were used for composite PLA + HA (PLA with 10% of HA) and PLA + BG (PLA with 10% of BG) scaffolds 3D printing. Produced scaffold morphology (pore sizes and threads heights/widths) was evaluated by SEM (Fig. 1 A): the mean pore size of the PLA scaffolds was 414.43 ± 23.4 μm, with the filament height of 219.4 ± 8.4 μm and width of 387.9 ± 10.8 μm. The composite PLA + HA scaffolds had 412.3 ± 10.9 μm mean pore size with threads height of 224 ± 9.5 μm and width 407.6 ± 17.9 μm. In the PLA + BS composite 3D printed scaffolds, filaments height was 218 ± 10.2 μm and width was 384.4 ± 13.0 μm, which formed about 396.9 ± 25.5 μm size pores (Fig. 1B). Moreover, the obtained SEM micrographs show that BG and HA particles are evenly distributed in the composite PLA + BG and PLA + HA filaments (Fig. 1A).

The impact of nonorganic components – HA and BG to scaffold water absorption and protein binding properties were evaluated. The results of water absorption revealed that both pure PLA and composite PLA + HA scaffolds tended to absorb less water than PLA + BG scaffold ($p < 0.01$) (Fig. 1C). The same tendency was observed in serum protein adsorption

to scaffold surface evaluation. The highest amount of deposited proteins was detected on PLA + BG scaffolds, compared to PLA ($p < 0.01$) and PLA + HA ($p < 0.05$) specimens (Fig. 1D).

3.2. DPSCs characterization

Cells were isolated from rat's incisors dental pulps. Surface antigens analysis by flow cytometry demonstrated that DPSCs were positive for CD44, CD54, CD90 and negative for hematopoietic and endothelial markers CD13, CD14 and CD31 (Fig. S1).

3.3. Cell adhesion on composite scaffolds

To compare bioceramic-polymers composites impacts on DPSCs adhesion efficiency, the cells were seeded on the tested composite scaffolds and cell surface area (0.5, 2 and 24 h post-seeding) was analysed by visualising DPSC F-actin filaments. Obtained F-actin filaments fluorescent microscope images (Fig. S2) and cell surface area measurements (Fig. 2B) showed that DPSCs were capable to adhere to all the tested surfaces. However, after 0.5 h, the cells adhere better to composite PLA + HA and PLA + BG scaffolds compared with pure PLA ($p < 0.01$ and $p < 0.05$ respectively). However, after 24 h the best DPSCs adhesion efficiency was observed on PLA scaffolds and the worst adhesion was determined on PLA + BG, compared with pure PLA ($p < 0.01$) and PLA + HA ($p < 0.001$). To understand better the cell adhesion process, focal adhesion spots (24 h post-seeding) were visualized (Fig. 2A) and quantified (Fig. 2C). The results showed that the minimum number of FA were formed in cells grown on composite PLA + BG scaffolds, which means that DPSC adhesion strength on PLA + BG scaffolds was the weakest compared to PLA + HA ($p < 0.05$) and pure PLA ($p < 0.05$).

3.4. DPSCs migration and proliferation on tested scaffolds

To evaluate the impact of the different chemical composition of scaffold filaments on cell attraction, vertical migration of DPSCs onto tested scaffolds was assessed (Fig. 3A). Composite scaffolds were incubated on a monolayer of DPSCs for 72 h, and then the amount of cells migrated onto these scaffolds was determined. The results indicated that among the tested scaffolds the most attractive for cells was composite PLA + BG surface, in this case, DPSCs demonstrated the highest migration potential compared to PLA ($p < 0.01$) and PLA + HA ($p < 0.01$).

To evaluate the influence of different composite materials to cell proliferative activity, DPSC number was registered at 24, 48, 72, 96 and 120 h after cell seeding. Results were standardized according to cell number determined on the appropriate composites after 24 h of incubation. The assessment of cell proliferation activity indicated that, almost after all time measurements, DPSCs showed significantly better proliferative activity on pure PLA scaffolds compared to composite ones (Fig. 3B). The worst DPSC proliferation was registered on the composite PLA + BG scaffolds. However, after 96 and 120 h, significant differences

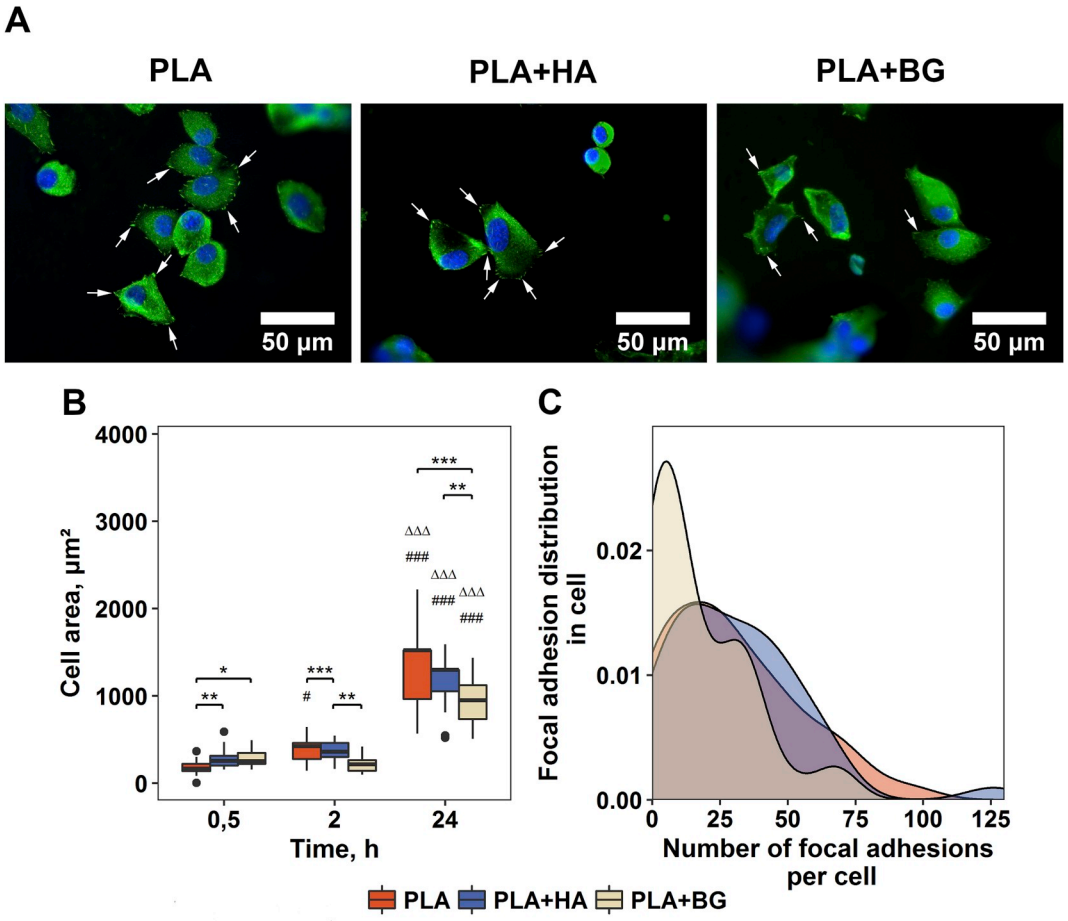

Fig. 2. DPSC adhesion on 3D printed composite scaffolds. A – immunofluorescence staining of nucleus (DAPI, blue) and FA spots (vinculin, green) in DPSCs after 24 h post seeding; B – cell surface area after culturing for 0.5, 2 and 24 h on the scaffolds; C – quantitative FA evaluation within the cells after culturing for 24 h. Statistically significant data between different scaffold groups are indicated as * ($p < 0.05$), ** ($p < 0.01$) and *** ($p < 0.001$), while # shows statistically significant differences compared to 0.5 h within the same scaffold group - # ($p < 0.05$), ### ($p < 0.001$), Δ demonstrates significant differences compared to 2 h within the same scaffold group - ΔΔΔ ($p < 0.001$).

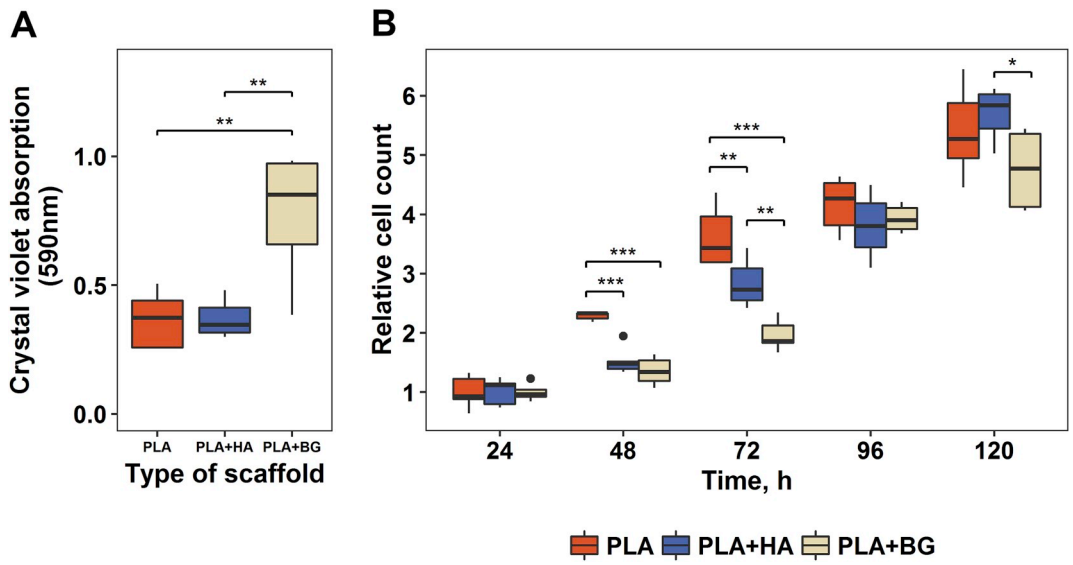

Fig. 3. DPSC migration and proliferation on tested scaffolds. A – Evaluation of vertical cell migration onto the composite scaffolds using crystal violet assay; B – relative DPSC proliferation rate; data is standardized according to the number of cells maintained on appropriate scaffolds for 24 h. Statistically significant results indicated as * ($p < 0.05$), ** ($p < 0.01$) and *** ($p < 0.001$).

between PLA and PLA + HA or PLA + BG scaffolds were not detected.

3.5. Osteogenic differentiation

To determine the effect of scaffolds' chemical composition on the induction of DPSC osteogenic differentiation, ALP activity, bone tissue specific ECM and osteogenic-related gene expression were analysed.

ALP activity results were normalised according to cell counts determined on each type of scaffold after predetermined time points. Obtained results indicated that ALP activity in DPSCs grown on composite PLA + BG scaffolds was increased even after 1st cultivation day, compared to pure PLA ($p < 0.01$) and PLA + HA ($p < 0.01$) (Fig. 4 A). Later on, ALP activity in DPSCs grown on PLA + BG scaffolds gradually decreased. However, the highest enzyme activity, in the cells maintained on PLA and PLA + HA scaffolds, was detected only after 10 days of differentiation (Fig. 4A).

DPSCs grown on all surfaces tended to accumulate collagen in their ECM, however, significant differences between scaffold impact on collagen accumulation were not observed (Fig. 4B). In contrast, ECM mineralisation results indicated that even at the 1st day of DPSC cultivation on tested scaffolds, higher calcium depositions were observed on both composite scaffolds (PLA + HA ($p < 0.001$) and PLA + BG ($p < 0.001$)) compared to pure PLA (Fig. 4C). Moreover, at 7 and 10 day of the differentiation, the greatest and statistically significant increase of ECM mineralisation was registered in cell cultures maintained on composite PLA + BG scaffolds.

Runx2, OPN, and OCN gene expression measurement results showed that all tested scaffolds stimulated DPSC differentiation towards osteogenic lineage by upregulation of Runx2 and OPN gene expression (Fig. 5A). Moreover, the highest Runx2 gene expression was determined in cells maintained on all tested scaffolds at 10th day of differentiation. In DPSCs grown on PLA + BG, it tended to increase greater compared to cells grown on pure PLA ($p < 0.27$) and PLA + HA ($p < 0.09$) scaffolds. However, in this case, differences in Runx2 gene expression did not reach statistically significant levels. In the case of OPN gene expression, it remained almost unchanged at 1st and 7th differentiation evaluation days in cells grown on all investigated scaffolds. Enhanced OPN expression after 10 days of culture was observed in cells maintained on PLA + BG scaffolds ($p < 0.01$) compared to PLA and PLA + HA groups (Fig. 5B). Differences in OCN gene expression were not observed on any time point in cells grown on tested scaffolds. At 10th day of DPSC differentiation, OCN showed a slightly higher increase in gene expression level in DPSCs grown on PLA + BG scaffold group compared to other ones (PLA – $p < 0.61$; PLA + HA – $p < 0.84$), but it did not reach significant values (Fig. 5C).

4. Discussion

Bone tissue engineering continues to gain more and more attention. It is a promising alternative for widely used autografts and allografts in bone defect reconstruction and repair procedures (T. and C., 2001). Currently, scientists are trying to create artificial bone tissue grafts from various natural and synthetic materials alone or in a combination with each other (Jammalamadaka et al., 2018; Narayanan et al., 2016). Over the last few years, artificial bone grafts manufactured from composite materials showed promising results. Many studies compare the properties of different kinds of scaffolds from various polymers and bio-ceramics combinations fabricated using diverse techniques (Huang et al., 2018; Kim et al., 2017). One of the promising artificial bone graft manufacture techniques is 3D printing and, considering potential chemical constitution, composite material (Burgio et al., 2018; Huang et al., 2018; Kim et al., 2017; Kuss et al., 2018; Qi et al., 2018; Zhang et al., 2016). 3D printing stands out from other scaffold manufacture methods since it is cheap, fast and suitable for highly structured scaffolds production. HA and BG bioceramics perfectly enrich the widely used polymers in 3D printing – PLA or PCL. It makes polymeric material more biocompatible, osteoconductive and even osteoinductive (Motealleh et al., 2017 n.d.; Zhang et al., 2016). However, there are no studies in which osteoconductive and osteoinductive properties of HA or BG and PLA composites scaffolds fabricated using 3D printing technique would be compared to each other. To determine, which composite material is the most suitable for the use in artificial bone grafts production by 3D printing technology, an *in vitro* study was carried out. The biological properties of composites PLA + HA and PLA + BG and their effect on DPSCs adhesion, migration, proliferation and osteogenesis were compared (Fig. 6).

Composite scaffold materials were produced by mixing pure PLA beads with HA or 45S5 BG particles (mass ratio 9:1). The composite filaments were fabricated using filament extruder. We used the maximal amount of the bioceramics, which still had mechanical properties compatible with FFF manufacturing method. Obtained filaments were used for 3D printing and finally, composite PLA + HA (PLA with 10% of

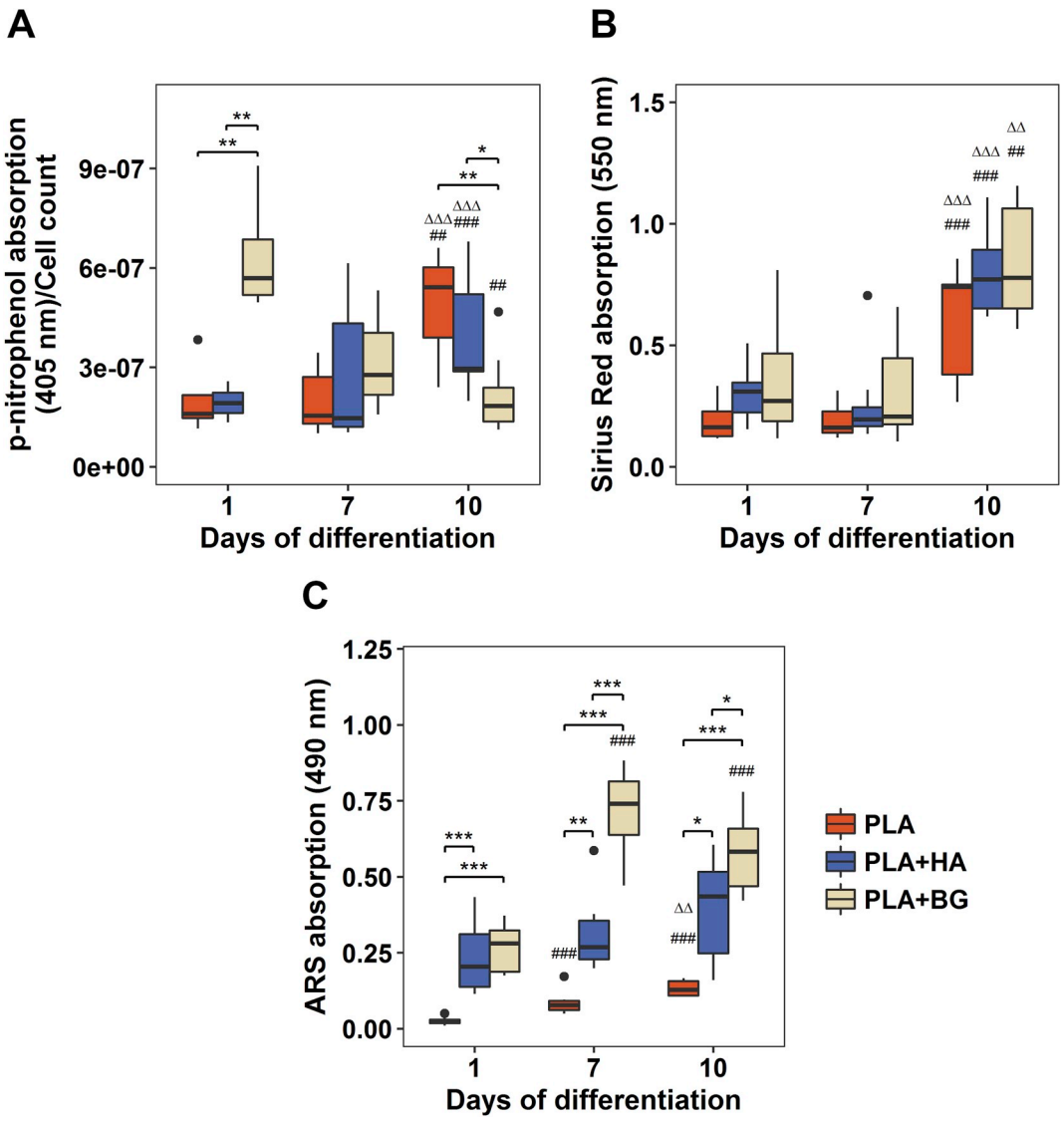

Fig. 4. Osteogenic differentiation assessment. A - ALP activity at 1, 7 and 10 days of osteogenic differentiation evaluated by p-nitro phenol assay; B - DPSCs collagen production evaluated by Sirius Red staining; C - ECM mineralisation analysis by ARS staining. Statistically significant differences between different scaffolds groups are marked with * ($p < 0.05$), ** ($p < 0.01$) and *** ($p < 0.001$), while # shows statistically significant differences compared to day 1 within the same scaffold group - ## ($p < 0.01$), ### ($p < 0.001$), Δ demonstrates significant differences compared to day 7 within the same scaffold group - ΔΔ ($p < 0.01$), ΔΔΔ ($p < 0.001$).

HA) and PLA + BG (PLA with 10% of BG) scaffolds were manufactured. SEM observations of the scaffolds showed that pure PLA specimens had a surface of continuous and smooth appearance, while the PLA + HA and PLA + BG scaffolds surfaces had visible HA or BG particles. Nevertheless, the HA particles were scattered more equally throughout scaffold surface compared to BG beads in their composites. All 3D printed PLA, PLA + HA and PLA + BS scaffolds had about 400 μm diameter interconnected pores, which, according to the literature, is a perfect topography for bone tissue regeneration (Ji et al., 2018).

For successful bone regeneration not only porous topography of bone graft is important. The constructed scaffold should also be as hydrophilic as possible. Implanted bone graft constantly interacts with body fluids, which are rich in nutrients and proteins. Good water absorption and hydrophilicity of the construct would ensure better nutrients and proteins absorption, which could lead to successful scaffold integration into the body (Ma et al., 2007). For this reason, the impact of nonorganic components (HA and BG) to scaffold water absorption properties was evaluated in our experiments. The results showed that BG components increased water absorption by about 15.5% more than pure PLA and PLA + HA scaffolds. It was shown previously that the incorporation of hydrophilic materials into hydrophobic polymers is a feasible approach to improve water absorption of these composites (Li and Chang, 2004; Wu et al., 2013). In our case, hydrophilic BG beads were more protruded from PLA filament than HA particles, which could lead to the formation of larger hydrophilic surface area on PLA + BG scaffold and as a result a better PLA + BG composite water absorption might have been achieved.

Artificial bone grafts must also be suitable and attractive for cells to adhere. Cell-surface interactions are necessary to maintain cell survival and homeostasis in newly formed tissue (Kutys et al., 2013; Ohashi et al., 2017). However, cells cannot directly attach to the synthetic polymer surface, because their surface molecules, such as integrins, can interact only with certain extracellular proteins' amino acid sequences. For this reason, it is necessary that the proteins, presented in the body fluids (such as albumin, α2-HS-glycoprotein and etc.) could easily adsorb and deposit on the scaffold surface (Aiyelabegan and Sadroddiny, 2017; Allen et al., 2006). Thus, we have determined that all our tested specimens' surfaces were suitable for proteins to adsorb. However, the highest amount of deposited proteins was determined on PLA + BG scaffold surface. In case of DPSC adhesion, cells showed the capability to adhere to all tested surfaces, since they acquired flatter morphology

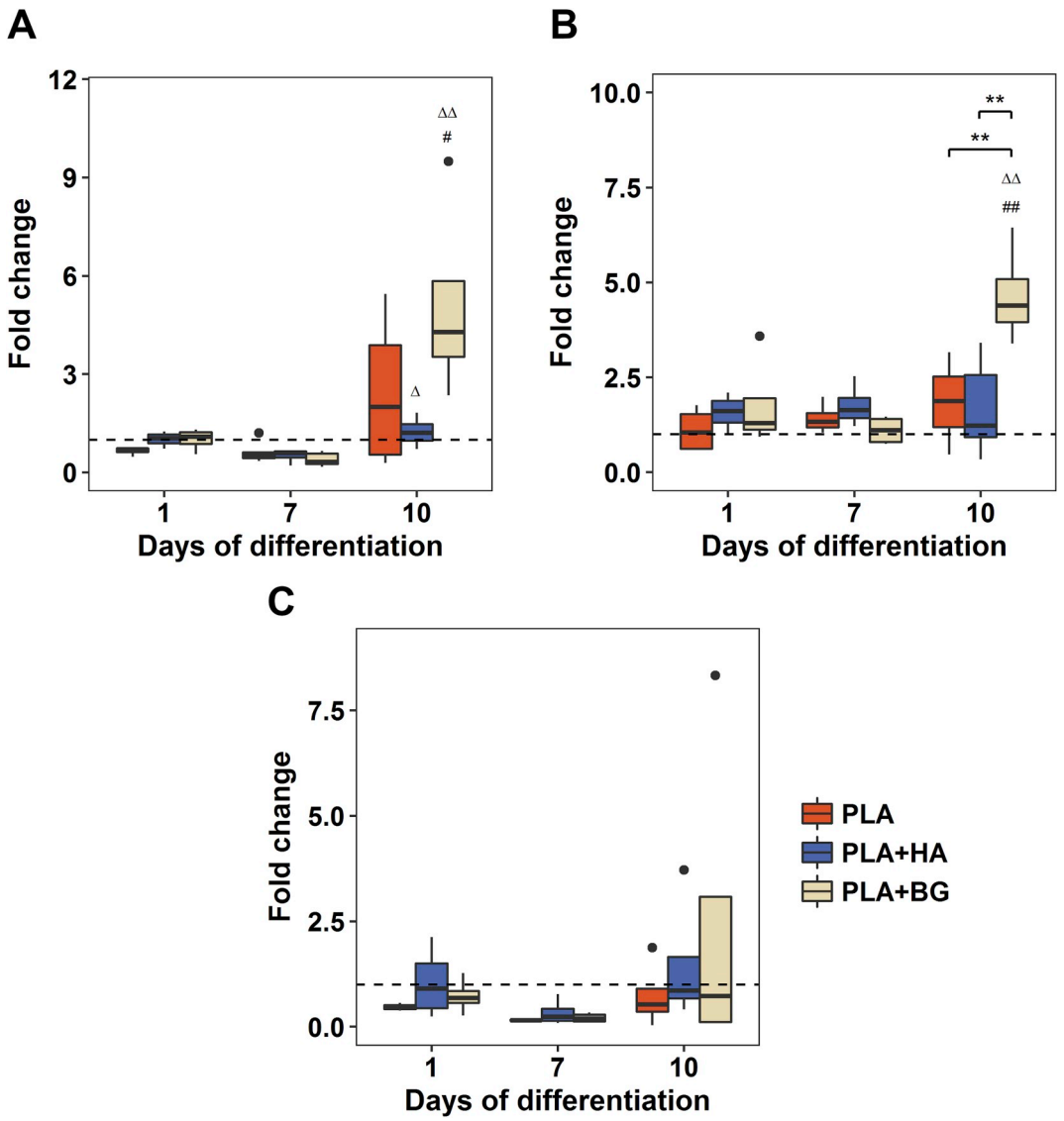

Fig. 5. Osteogenesis-related gene (Runx2, OPN, OCN) expression levels in DPSC grown on 3D printed scaffolds. A – Runx2, B – Osteopontin and C - Osteocalcin expression level changes during 10 days of cells cultivation on PLA and composite scaffolds. Statistically significant differences between cells grown on different scaffolds groups are marked with ** ($p < 0.01$), while # shows statistically significant differences compared to day 1 within the same scaffold group - # ($p < 0.05$), ## ($p < 0.01$), Δ demonstrates a significant differences compared to day 7 within the same scaffold group - ΔΔ ($p < 0.01$).

after 24 h of cultivation compared to 0.5 and 2 h. However, contrary to protein adsorption results, different scaffold groups' adhesion efficiency and strength comparison showed that the worst DPSC adhesion was observed on composite PLA + BG scaffolds. In this scaffold group, the changes in cell surface area within 24 h were minimal and the determined focal adhesions counts within the cells were the lowest. As mentioned before, cells can only attach to surfaces containing deposited proteins from the medium or body fluids. The interaction between proteins and PLA + HA or PLA + BG surface is primarily facilitated by coordinate covalent and electrostatic bonds. For example, electrostatic interactions could occur between the negatively charged ions (in BG) or phosphorus groups (in HA) surface and protonated amine groups (–NH) of proteins, thus high surface charge density of the ions or phosphorus of BG and HA surfaces induce strong protein adsorption (Einspahr and Bugg, 1974; Gorbunoff and Timasheff, 1984; Lobel and Hench, 1996; Srinivasan et al., 2012). Therefore, BG containing scaffolds should have better interaction with cells compared to pure PLA or PLA + HA scaffolds. Conversely, BG beads had a negative effect on cell attachment in the first 24 h of cell incubation onto the surfaces.

To achieve successful bone tissue regeneration, endogenous stem cells should be able to migrate to the damaged tissue site, where they can proliferate, synthesize new ECM, and in that way replace artificial bone scaffold and form fully functional tissue (Su et al., 2018). Therefore, a promising tissue-engineered bone graft should attract and stimulate cells to migrate and proliferate. For this purpose, scaffold surfaces are often modified by various cytokines or ECM proteins to promote cell migration and proliferation onto artificially created bone graft (Ohashi et al., 2017; Su et al., 2018). However, as shown previously, scaffold chemistry and topography properties are sufficient enough to modulate cell migration and proliferation (Anselme, 2000; Tamburaci and Tihminlioglu, 2018). For this reason, the migration of DPSCs onto composite scaffolds was analysed. It was shown that the most intensive cell migration was promoted by PLA + BG scaffolds compared to pure PLA and PLA + HA. These results can be caused by dissolved ions from 45S5 BG, which stimulate cell migration (Li et al., 2016; Yu et al., 2016). However, during the DPSCs proliferation evaluation, it was observed that cells cultivated on pure PLA scaffolds proliferate better compared to both composite scaffolds groups. Such slower cell proliferation could be associated with the onset of DPSC osteogenic differentiation on these composite scaffolds. It is well known that stem cells committed to

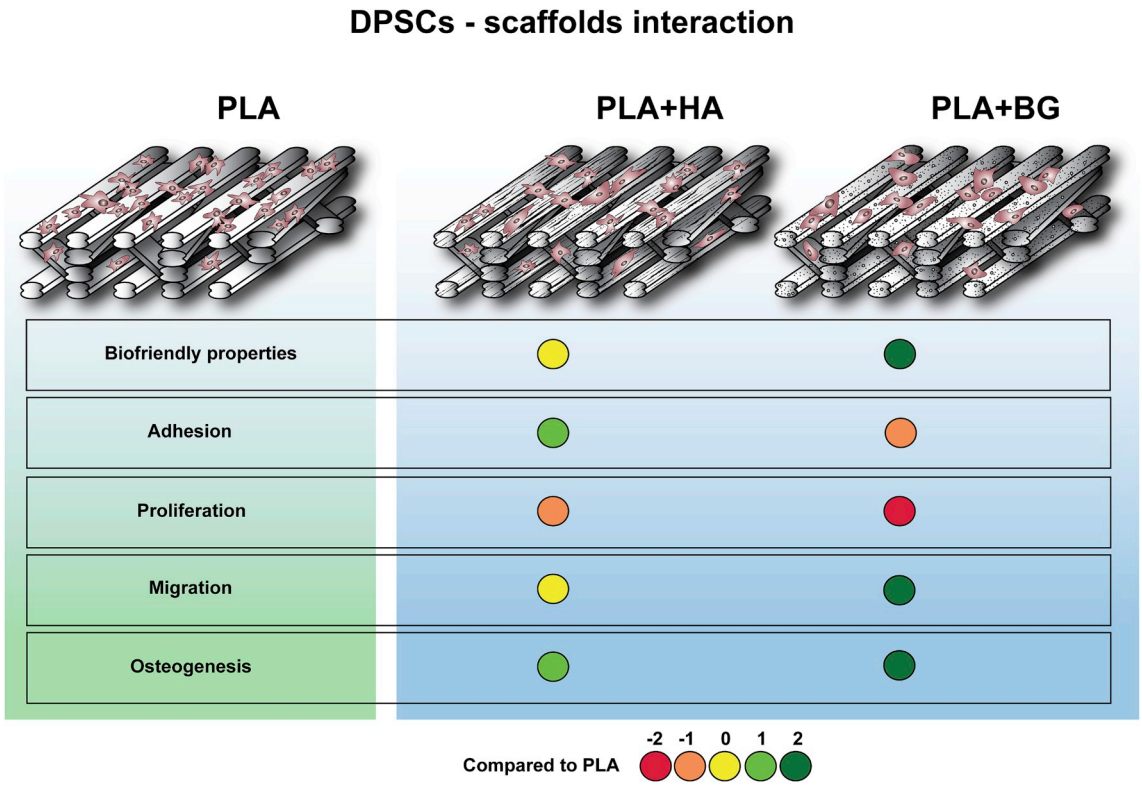

Fig. 6. Comparison of PLA + HA and PLA + BG scaffolds osteoinductive, osteoconductive and biofriendly properties.

differentiate into the specific lineage exit the cell cycle and start the differentiation process within the cell (Rutkovskiy et al., 2016).

Osteoinductivity is another important feature of the scaffold designed for bone regeneration. One of the main bone tissue engineering goals is to create an artificial bone graft which, solely by its chemical composition and topographic surface characteristics, would initiate spontaneous stem cell osteogenic differentiation (Alizadeh-Osgouei et al., 2019; Gómez-Cerezo et al., 2019; Jaidev and Chatterjee, 2019; Jiang et al., 2012). In order to compare which of the bioceramics (HA or BG) demonstrates better osteoinductivity properties, ALP activity, bone tissue specific ECM and osteogenesis-related gene expression were analysed in DPSCs cultivated on PLA + HA as well as PLA + BG composite scaffolds. ALP is an early marker for bone repair and regeneration, which is expressed in osteogenic-differentiation committed cells (Kuru et al., 1999). Results obtained from our study indicated that PLA + BG scaffolds induced the earliest and highest increase in ALP activity compared to pure PLA and PLA + HA samples. Moreover, to elucidate scaffold-triggered bone-specific ECM deposition, collagen and calcium production were analysed. It is known that stem cells, committed to osteogenic lineage, produce and accumulate ECM rich in type I collagen and calcium mineral deposits (Langenbach and Handschel, 2013; Rutkovskiy et al., 2016). Our results indicated that the highest ECM mineralisation efficiency was registered when cells were grown on the composite PLA + BG scaffolds which correlated with ALP activity results. However, all the analysed scaffold groups did not have a significant impact on the collagen accumulation process as differences between them were not observed. To further confirm the enhanced osteogenic activity of the composite PLA + BG scaffolds, mRNA expression of osteogenesis-related genes (Runx2, OPN, and OCN) in DPSCs were evaluated. It was observed that, on all the tested samples, the expression of Runx2 and OPN genes were up-regulated at 10th day of differentiation. We believe that the BG chemical composition could affect the biological response of DPSCs due to the dissolution of ions from BG particles. Studies have shown that the released Ca, P and Si ions from BG can stimulate metabolic activity, proliferation and differentiation of osteoblasts (Qi et al., 2018; Silver et al., 2001; Valerio et al., 2004; Xynos et al., 2001). Besides, the highest Runx2 and OPN genes expression was determined in cells grown on PLA + BG scaffolds; this confirms that this particular composite group ensures strongest osteoinductivity. In contrast, there was no significant increase in OCN gene expression in DPSCs cultivated on tested specimens. OCN is an ECM protein, which is also a specific marker for mature osteoblasts. It was shown that physical environment induces only primary differentiation steps in stem cells (Lee et al., 2015). Chemical inductors or additional time is needed for cells to reach the final stage of differentiation (Tanaka et al., 2009). This was also observed in our study. The lack of OCN expression after 10 days of spontaneous DPSCs differentiation on tested scaffolds, despite ECM mineralisation, concludes that cells are not fully matured yet.

Both PLA + HA and PLA + BS composites had positive effect on DPSC osteogenesis. The cells maintained on these scaffolds demonstrate enhanced expression of osteogenic differentiation markers. As a consequence, stronger cell osteogenic lineage commitment impacted DPSC proliferation and morphology (Fig. 6). Cell proliferation is usually negatively affected by their differentiation (Cooper, 2000; Janners and Searls, 1970; Li and Kirschner, 2014).

Even though both bioceramics had a positive effect to cell osteogenesis, their impact on cell behavior was different. Cell spreading and higher numbers of formed FA were observed on PLA + HA scaffolds compered to PLA + BG. However, this might be caused by higher DPSC migration on PLA + BG scaffolds. Intermediate level of attachment strength produces maximal migration rates (DiMilla et al., 1991). At low adhesive strength sufficient traction cannot be generated for cell migration to proceed, whereas, at higher adhesive strength, the cells do not release their adhesions efficiently (Huttenlocher et al., 1995). Thus, this explains why DPSCs have formed a smaller amount of FA compared to PLA + HA scaffolds.

Osteogenic differentiation data revealed that DPSCs grown on the PLA + BG composites even after first days of cultivation showed increased expression of genes related to bone lineage differentiation and

enzymatic ALP activity. Although both HA and BG had a positive effect to collagen production, more mineralised ECM was observed on PLA + BG scaffolds. Also, earlier DPSC osteogenic commitment on the PLA + BG scaffolds was in agreement with slower cell proliferation on BG containing scaffolds (Ruijtenberg and van den Heuvel, 2016).

5. Conclusions

The results showed that BG particles, in comparison to HA, are more suitable for the production of 3D printed composite scaffolds for bone regeneration. Our fabricated PLA + BG composite scaffold demonstrated better biofriendly and osteoinductive properties compared to pure PLA and PLA + HA scaffolds, revealing strong BG bioceramic advantage against HA. It is likely that BG chemical composition is the main factor determining this difference of effect between PLA + HA and PLA + BG. Ions dissociated from BG particles affected cell fate, biological response, and osteogenic commitment more than HA, which only ensures inorganic bone building material accessibility.

Finally, tested PLA + BG composition was compatible with FFF 3D printing application. 3D printing technology in combination with easily accessible medical grade PLA and BG materials allows the production of patient-specific, cheap, effective and quick to manufacture scaffolds for clinical applications for bone defect treatment.

Data availability

The data will be made available on request.

Declaration of competing interest

We declare no competing interests.

CRediT authorship contribution statement

Milda Alksne: Investigation, Methodology, Formal analysis, Writing - original draft, Writing - review & editing. **Migle Kalvaityte:** Investigation, Formal analysis. **Egidijus Simoliunas:** Formal analysis, Writing - original draft, Writing - review & editing. **Ieva Rinkunaite:** Visualization. **Ieva Gendviliene:** Methodology. **Janis Locs:** Resources. **Vygandas Rutkunas:** Conceptualization. **Virginija Bukelskiene:** Supervision, Writing - original draft, Writing - review & editing.

Acknowledgements

This work was supported by the grant from the Research Council of Lithuania [Project No. MIP – 046/2015] and L'ORÉAL Baltic "For Women in Science" fellowship with the support of the Lithuanian National Commission for UNESCO and the Lithuanian Academy of Sciences. Synthesis of hydroxyapatite at Riga Technical University was done with the support of "Development of nanostructured bone substitute materials and study of immunological aspects in bone tissue regeneration" project [Project No. RTU/RSU-17].

Appendix A. Supplementary data

Supplementary data to this article can be found online at https://doi.org/10.1016/j.jmbbm.2020.103641.

References

Aiyelabegan, H.T., Sadroddiny, E., 2017. Fundamentals of protein and cell interactions in biomaterials. Biomed. Pharmacother. 88, 956–970. https://doi.org/10.1016/j.biopha.2017.01.136.

Alconcel, S.N.S., Baas, A.S., Maynard, H.D., 2011. FDA-approved poly(ethylene glycol)–protein conjugate drugs. Polym. Chem. 2, 1442. https://doi.org/10.1039/c1py00034a.

Alizadeh-Osgouei, M., Li, Y., Wen, C., 2019. A comprehensive review of biodegradable synthetic polymer-ceramic composites and their manufacture for biomedical applications. Bioact. Mater. 4, 22–36. https://doi.org/10.1016/j.bioactmat.2018.11.003.

Alksne, M., Simoliunas, E., Kalvaityte, M., Skliutas, E., Rinkunaite, I., Gendviliene, I., Baltriukiene, D., Rutkunas, V., Bukelskiene, V., 2019. The effect of larger than cell diameter polylactic acid surface patterns on osteogenic differentiation of rat dental pulp stem cells. J. Biomed. Mater. Res. A 107. https://doi.org/10.1002/jbm.a.36547.

Allen, L.T., Tosetto, M., Miller, I.S., O'Connor, D.P., Penney, S.C., Lynch, I., Keenan, A.K., Pennington, S.R., Dawson, K.A., Gallagher, W.M., 2006. Surface-induced changes in protein adsorption and implications for cellular phenotypic responses to surface interaction. Biomaterials 27, 3096–3108. https://doi.org/10.1016/j.biomaterials.2006.01.019.

Anselme, K., 2000. Osteoblast adhesion on biomaterials. Biomaterials 21, 667–681.

T, A., C, J., 2001. Osteoinduction, osteoconduction and osseointegration. Eur. Spine J. 10, S96–S101. https://doi.org/10.1007/s005860100282.

Baino, F., Novajra, G., Vitale-Brovarone, C., 2015. Bioceramics and scaffolds: a winning combination for tissue engineering. Front. Bioeng. Biotechnol. 3, 202. https://doi.org/10.3389/fbioe.2015.00202.

Barbeck, M., Serra, T., Booms, P., Stojanovic, S., Najman, S., Engel, E., Sader, R., Kirkpatrick, C.J., Navarro, M., Ghanaati, S., 2017. Analysis of the in vitro degradation and the in vivo tissue response to bi-layered 3D-printed scaffolds combining PLA and biphasic PLA/bioglass components – guidance of the inflammatory response as basis for osteochondral regeneration. Bioact. Mater. 2, 208–223. https://doi.org/10.1016/j.bioactmat.2017.06.001.

Berebichez-Fridman, R., Montero-Olvera, P.R., 2018. Sources and clinical applications of mesenchymal stem cells: state-of-the-art review. Sultan Qaboos Univ. Med. J. 18, e264–e277. https://doi.org/10.18295/squmj.2018.18.03.002.

Böstman, O., Pihlajamäki, H., 2000. Clinical biocompatibility of biodegradable orthopaedic implants for internal fixation: a review. Biomaterials 21, 2615–2621. https://doi.org/10.1016/s0142-9612(00)00129-0.

Burgio, F., Rimmer, N., Pieles, U., Buschmann, J., Beaufils-Hugot, M., 2018. Characterization and in ovo vascularization of a 3D-printed hydroxyapatite scaffold with different extracellular matrix coatings under perfusion culture. Biol. Open 7, bio034488. https://doi.org/10.1242/bio.034488.

Cao, W., Hench, L.L., 1996. Bioactive materials. Ceram. Int. 22, 493–507. https://doi.org/10.1016/0272-8842(95)00126-3.

Chen, W., Zhou, H., Tang, M., Weir, M.D., Bao, C., Xu, H.H.K., 2012. Gas-foaming calcium phosphate cement scaffold encapsulating human umbilical cord stem cells. Tissue Eng. A 18, 816–827. https://doi.org/10.1089/ten.TEA.2011.0267.

Chen, X., Fan, H., Deng, X., Wu, L., Yi, T., Gu, L., Zhou, C., Fan, Y., Zhang, X., 2018. Scaffold structural microenvironmental cues to guide tissue regeneration in bone tissue applications. Nanomaterials 8, 960. https://doi.org/10.3390/nano8110960.

Chen, X., Gao, C., Jiang, J., Wu, Y., Zhu, P., Chen, G., 2019. 3D printed porous PLA/nHA composite scaffolds with enhanced osteogenesis and osteoconductivity in vivo for bone regeneration. Biomed. Mater. 14, 065003 https://doi.org/10.1088/1748-605X/ab388d.

Chong, S.-F., Smith, A.A.A., Zelikin, A.N., 2013. Microstructured, functional PVA hydrogels through bioconjugation with oligopeptides under physiological conditions. Small 9, 942–950. https://doi.org/10.1002/smll.201201774.

Conoscenti, G., Carrubba, V. La, Brucato, V., 2017. A Versatile Technique to Produce Porous Polymeric Scaffolds: the Thermally Induced Phase Separation (TIPS) Method. https://doi.org/10.21767/2572-4657.100012.

Cooper, G.M., 2000. Cell Proliferation in Development and Differentiation.

De Witte, T.-M., Fratila-Apachitei, L.E., Zadpoor, A.A., Peppas, N.A., 2018. Bone tissue engineering via growth factor delivery: from scaffolds to complex matrices. Regen. Biomater. 5, 197–211. https://doi.org/10.1093/rb/rby013.

Delabarde, C., Plummer, C.J.G., Bourban, P.E., Månson, J.A.E., 2011. Accelerated ageing and degradation in poly-L-lactide/hydroxyapatite nanocomposites. Polym. Degrad. Stab. 96, 595–607. https://doi.org/10.1016/j.polymdegradstab.2010.12.018.

Deng, X., Hao, J., Wang, C., 2001. Preparation and mechanical properties of nanocomposites of poly(D,L-lactide) with Ca-deficient hydroxyapatite nanocrystals. Biomaterials 22, 2867–2873.

DiMilla, P.A., Barbee, K., Lauffenburger, D.A., 1991. Mathematical model for the effects of adhesion and mechanics on cell migration speed. Biophys. J. 60, 15–37. https://doi.org/10.1016/S0006-3495(91)82027-6.

Dorati, R., DeTrizio, A., Modena, T., Conti, B., Benazzo, F., Gastaldi, G., Genta, I., 2017. Biodegradable scaffolds for bone regeneration combined with drug-delivery systems in osteomyelitis therapy. Pharmaceuticals 10. https://doi.org/10.3390/ph10040096.

Einspahr, H., Bugg, C.E., 1974. Calcium-binding to n-amino acids: crystal structure of calcium L-glutamate trihydrate. Acta Crystallogr. B30, 1037–1043. https://doi.org/10.1107/S0567740874004225.

Gómez-Cerezo, N., Casarrubios, L., Saiz-Pardo, M., Ortega, L., de Pablo, D., Díaz-Güemes, I., Fernández-Tomé, B., Enciso, S., Sánchez-Margallo, F.M., Portolés, M.T., Arcos, D., Vallet-Regí, M., 2019. Mesoporous bioactive glass/ϵ-polycaprolactone scaffolds promote bone regeneration in osteoporotic sheep. Acta Biomater. https://doi.org/10.1016/J.ACTBIO.2019.04.019.

Gorbunoff, M.J., Timasheff, S.N., 1984. The interaction of proteins with hydroxyapatite: III. Mechanism. Anal. Biochem. 136, 440–445. https://doi.org/10.1016/0003-2697(84)90241-0.

Gregor, A., Filová, E., Novák, M., Kronek, J., Chlup, H., Buzgo, M., Blahnová, V., Lukášová, V., Bartoš, M., Nečas, A., Hošek, J., 2017. Designing of PLA scaffolds for bone tissue replacement fabricated by ordinary commercial 3D printer. J. Biol. Eng. 11, 31. https://doi.org/10.1186/s13036-017-0074-3.

Gronthos, S., Brahim, J., Li, W., Fisher, L.W., Cherman, N., Boyde, A., DenBesten, P., Robey, P.G., Shi, S., 2002. Stem cell properties of human dental pulp stem cells. J. Dent. Res. 81, 531–535. https://doi.org/10.1177/154405910208100806.

Hannink, G., Arts, J.J.C., 2011. Bioresorbability, porosity and mechanical strength of bone substitutes: what is optimal for bone regeneration? Injury 42, S22–S25. https://doi.org/10.1016/j.injury.2011.06.008.

Huang, B., Caetano, G., Vyas, C., Blaker, J.J., Diver, C., Bártolo, P., 2018. Polymer-Ceramic Composite Scaffolds: the Effect of Hydroxyapatite and β-tri-Calcium Phosphate, vol. 11. Mater., Basel, Switzerland https://doi.org/10.3390/ma11010129.

Huttenlocher, A., Sandborg, R.R., Horwitz, A.F., 1995. Adhesion in cell migration. Curr. Opin. Cell Biol. 7, 697–706. https://doi.org/10.1016/0955-0674(95)80112-X.

Jaidev, L.R., Chatterjee, K., 2019. Surface functionalization of 3D printed polymer scaffolds to augment stem cell response. Mater. Des. 161, 44–54. https://doi.org/10.1016/J.MATDES.2018.11.018.

Jammalamadaka, U., Tappa, K., Jammalamadaka, U., Tappa, K., 2018. Recent advances in biomaterials for 3D printing and tissue engineering. J. Funct. Biomater. 9, 22. https://doi.org/10.3390/jfb9010022.

Janners, M.Y., Searls, R.L., 1970. Changes in rate of cellular proliferation during the differentiation of cartilage and muscle in the mesenchyme of the embryonic chick wing. Dev. Biol. 23, 136–165. https://doi.org/10.1016/S0012-1606(70)80011-2.

Jeong, J., Kim, J.H., Shim, J.H., Hwang, N.S., Heo, C.Y., 2019. Bioactive calcium phosphate materials and applications in bone regeneration. Biomater. Res. https://doi.org/10.1186/s40824-018-0149-3.

Ji, K., Wang, Y., Wei, Q., Zhang, K., Jiang, A., Rao, Y., Cai, X., 2018. Application of 3D printing technology in bone tissue engineering. Bio-Des. Manuf. 1, 203–210. https://doi.org/10.1007/s42242-018-0021-2.

Jiang, W., Shi, J., Li, W., Sun, K., 2012. Three dimensional melt-deposition of polycaprolactone/bio-derived hydroxyapatite composite into scaffold for bone repair. https://doi.org/10.1080/09205063.2012.698894.

Jiang, J., Hao, W., Li, Y., Yao, J., Shao, Z., Li, H., Yang, J., Chen, S., 2013. Hydroxyapatite/regenerated silk fibroin scaffold-enhanced osteoinductivity and osteoconductivity of bone marrow-derived mesenchymal stromal cells. Biotechnol. Lett. 35, 657–661. https://doi.org/10.1007/s10529-012-1121-2.

Jing, X., Mi, H.-Y., Turng, L.-S., 2017. Comparison between PCL/hydroxyapatite (HA) and PCL/halloysite nanotube (HNT) composite scaffolds prepared by co-extrusion and gas foaming. Mater. Sci. Eng. C 72, 53–61. https://doi.org/10.1016/J.MSEC.2016.11.049.

Jones, J.R., Lin, S., Yue, S., Lee, P.D., Hanna, J.V., Smith, M.E., Newport, R.J., 2010. Bioactive glass scaffolds for bone regeneration and their hierarchical characterisation. Proc. Inst. Mech. Eng. H 224, 1373–1387. https://doi.org/10.1243/09544119JEIM836.

Karageorgiou, V., Kaplan, D., 2005. Porosity of 3D biomaterial scaffolds and osteogenesis. Biomaterials 26, 5474–5491. https://doi.org/10.1016/j.biomaterials.2005.02.002.

Kasuga, T., Ota, Y., Nogami, M., Abe, Y., 2000. Preparation and mechanical properties of polylactic acid composites containing hydroxyapatite fibers. Biomaterials 22, 19–23. https://doi.org/10.1016/S0142-9612(00)00091-0.

Khanna-Jain, R., Vanhatupa, S., Vuorinen, A., S, G.K.B., Suuronen, R., Mannerstrom, B., Miettinen, S., 2012. Growth and differentiation of human dental pulp stem cells maintained in fetal bovine serum, human serum and serum-free/xeno-free culture media. J. Stem Cell Res. Ther. 2 https://doi.org/10.4172/2157-7633.1000126.

Kim, S.-S., Sun Park, M., Jeon, O., Yong Choi, C., Kim, B.-S., 2006. Poly(lactide-co-glycolide)/hydroxyapatite composite scaffolds for bone tissue engineering. Biomaterials 27, 1399–1409. https://doi.org/10.1016/J.BIOMATERIALS.2005.08.016.

Kim, J.-W., Shin, K.-H., Koh, Y.-H., Hah, M.J., Moon, J., Kim, H.-E., 2017. Production of Poly(ε-Caprolactone)/Hydroxyapatite Composite Scaffolds with a Tailored Macro/Micro-Porous Structure, High Mechanical Properties, and Excellent Bioactivity, vol. 10. Mater., Basel, Switzerland https://doi.org/10.3390/ma10101123.

Ko, E., Yang, K., Shin, J., Cho, S.-W., 2013. Polydopamine-assisted osteoinductive peptide immobilization of polymer scaffolds for enhanced bone regeneration by human adipose-derived stem cells. Biomacromolecules 14, 3202–3213. https://doi.org/10.1021/bm4008343.

Kuru, L., Griffiths, G.S., Petrie, A., Olsen, I., 1999. Alkaline phosphatase activity is up regulated in regenerating human periodontal cells. J. Periodontal. Res. 34, 123–127. https://doi.org/10.1111/j.1600-0765.1999.tb02231.x.

Kuss, M.A., Wu, S., Wang, Y., Untrauer, J.B., Li, W., Lim, J.Y., Duan, B., 2018. Prevascularization of 3D printed bone scaffolds by bioactive hydrogels and cell co-culture. J. Biomed. Mater. Res. B Appl. Biomater. 106, 1788–1798. https://doi.org/10.1002/jbm.b.33994.

Kutys, M.L., Doyle, A.D., Yamada, K.M., 2013. Regulation of cell adhesion and migration by cell-derived matrices. Exp. Cell Res. 319, 2434–2439. https://doi.org/10.1016/j.yexcr.2013.05.030.

Lam, C.X., Mo, X., Teoh, S., Hutmacher, D., 2002. Scaffold development using 3D printing with a starch-based polymer. Mater. Sci. Eng. C 20, 49–56. https://doi.org/10.1016/S0928-4931(02)00012-7.

Langenbach, F., Handschel, J., 2013. Effects of dexamethasone, ascorbic acid and ?-glycerophosphate on the osteogenic differentiation of stem cells in vitro. Stem Cell Res. Ther. 4, 117. https://doi.org/10.1186/scrt328.

Lee, J., Abdeen, A.A., Kilian, K.A., 2015. Rewiring mesenchymal stem cell lineage specification by switching the biophysical microenvironment. Sci. Rep. 4, 5188. https://doi.org/10.1038/srep05188.

Li, H., Chang, J., 2004. Fabrication and characterization of bioactive wollastonite/PHBV composite scaffolds. Biomaterials 25, 5473–5480. https://doi.org/10.1016/j.biomaterials.2003.12.052.

Li, V.C., Kirschner, M.W., 2014. Molecular ties between the cell cycle and differentiation in embryonic stem cells. Proc. Natl. Acad. Sci. U.S.A. 111, 9503–9508. https://doi.org/10.1073/pnas.1408638111.

Li, W., Wang, H., Ding, Y., Scheithauer, E.C., Goudouri, O.-M., Grünewald, A., Detsch, R., Agarwal, S., Boccaccini, A.R., 2015. Antibacterial 45S5 Bioglass®-based scaffolds reinforced with genipin cross-linked gelatin for bone tissue engineering. J. Mater. Chem. B 3, 3367–3378. https://doi.org/10.1039/C5TB00044K.

Li, H., He, J., Yu, H., Green, C.R., Chang, J., 2016. Bioglass promotes wound healing by affecting gap junction connexin 43 mediated endothelial cell behavior. Biomaterials 84, 64–75. https://doi.org/10.1016/J.BIOMATERIALS.2016.01.033.

Lin, L., Chow, K.L., Leng, Y., 2009. Study of hydroxyapatite osteoinductivity with an osteogenic differentiation of mesenchymal stem cells. J. Biomed. Mater. Res. A 89A, 326–335. https://doi.org/10.1002/jbm.a.31994.

Livak, K.J., Schmittgen, T.D., 2001. Analysis of relative gene expression data using real-time quantitative PCR and the 2-ΔΔCT method. Methods 25, 402–408. https://doi.org/10.1006/meth.2001.1262.

Lobel, K.D., Hench, L.L., 1996. In-vitro protein interactions with a bioactive gel-glass. J. Sol. Gel Sci. Technol. 7, 69–76. https://doi.org/10.1007/BF00401885.

Lopes, M.S., Jardini, A.L., Filho, R.M., 2012. Poly (lactic acid) production for tissue engineering applications. Procedia Eng. 42, 1402–1413. https://doi.org/10.1016/J.PROENG.2012.07.534.

Lowry, K.J., Hamson, K.R., Bear, L., Peng, Y.B., Calaluce, R., Evans, M.L., Anglen, J.O., Allen, W.C., 1997. Polycaprolactone/glass bioabsorbable implant in a rabbit humerus fracture model. J. Biomed. Mater. Res. 36, 536–541. https://doi.org/10.1002/(SICI)1097-4636(19970915)36:4<536::AID-JBM12>3.0.CO;2-8.

Luo, Y., Lin, Z., Guo, G., 2019. Biodegradation assessment of poly (lactic acid) filled with functionalized titania nanoparticles (PLA/TiO 2) under compost conditions. Nanoscale Res. Lett. 14 https://doi.org/10.1186/s11671-019-2891-4.

Ma, Z., Mao, Z., Gao, C., 2007. Surface modification and property analysis of biomedical polymers used for tissue engineering. Colloids Surfaces B Biointerfaces 60, 137–157. https://doi.org/10.1016/j.colsurfb.2007.06.019.

Malinauskas, M., Rekštytė, S., Lukoševičius, L., Butkus, S., Balčiūnas, E., Pečiukaitytė, M., Baltriukienė, D., Bukelskienė, V., Butkevičius, A., Kucevičius, P., Rutkūnas, V., Juodkazis, S., Malinauskas, M., Rekštytė, S., Lukoševičius, L., Butkus, S., Balčiūnas, E., Pečiukaitytė, M., Baltriukienė, D., Bukelskienė, V., Butkevičius, A., Kucevičius, P., Rutkūnas, V., Juodkazis, S., 2014. 3D microporous scaffolds manufactured via combination of fused filament fabrication and Direct laser writing ablation. Micromachines 5, 839–858. https://doi.org/10.3390/mi5040839.

Mao, D., Li, Q., Li, D., Chen, Y., Chen, X., Xu, X., 2018. Fabrication of 3D porous poly (lactic acid)-based composite scaffolds with tunable biodegradation for bone tissue engineering. Mater. Des. 142, 1–10. https://doi.org/10.1016/J.MATDES.2018.01.016.

Marra, K.G., Szem, J.W., Kumta, P.N., DiMilla, P.A., Weiss, L.E., 1999. In vitro analysis of biodegradable polymer blend/hydroxyapatite composites for bone tissue engineering. J. Biomed. Mater. Res. 47, 324–335. https://doi.org/10.1002/(SICI)1097-4636(19991205)47:3<324::AID-JBM6>3.0.CO;2-Y.

Monterubbianesi, R., Bencun, M., Pagella, P., Woloszyk, A., Orsini, G., Mitsiadis, T.A., 2019. A comparative in vitro study of the osteogenic and adipogenic potential of human dental pulp stem cells, gingival fibroblasts and foreskin fibroblasts. Sci. Rep. 9, 1761. https://doi.org/10.1038/s41598-018-37981-x.

Motealleh, A., Eqtesadi, S., Civantos, A., Pajares, A., Miranda, P., 2017. Robocast 45S5 bioglass scaffolds: in vitro behavior. J. Mater. Sci. 52, 9179–9191. https://doi.org/10.1007/s10853-017-0775-5.

Myung, S.W., Ko, Y.M., Kim, B.H., 2014. Protein adsorption and cell adhesion on three-dimensional polycaprolactone scaffolds with respect to plasma modification by etching and deposition techniques. Jpn. J. Appl. Phys. 53 https://doi.org/10.7567/JJAP.53.11RB01, 11RB01.

Narayanan, G., Vernekar, V.N., Kuyinu, E.L., Laurencin, C.T., 2016. Poly (lactic acid)-based biomaterials for orthopaedic regenerative engineering. Adv. Drug Deliv. Rev. 107, 247–276. https://doi.org/10.1016/j.addr.2016.04.015.

Noda, S., Kawashima, N., Yamamoto, M., Hashimoto, K., Nara, K., Sekiya, I., Okiji, T., 2019. Effect of cell culture density on dental pulp-derived mesenchymal stem cells with reference to osteogenic differentiation. Sci. Rep. 9, 5430. https://doi.org/10.1038/s41598-019-41741-w.

Ohashi, K., Fujiwara, S., Mizuno, K., 2017. Roles of the cytoskeleton, cell adhesion and rho signalling in mechanosensing and mechanotransduction. J. Biochem. 161, mvw082. https://doi.org/10.1093/jb/mvw082.

Pei, B., Wang, W., Fan, Y., Wang, X., Watari, F., Li, X., 2017. Fiber-reinforced scaffolds in soft tissue engineering. Regen. Biomater. 4, 257–268. https://doi.org/10.1093/rb/rbx021.

Polini, A., Pisignano, D., Parodi, M., Quarto, R., Scaglione, S., 2011. Osteoinduction of human mesenchymal stem cells by bioactive composite scaffolds without supplemental osteogenic growth factors. PLoS One 6, e26211. https://doi.org/10.1371/journal.pone.0026211.

Potdar, P.D., Jethmalani, Y.D., 2015. Human dental pulp stem cells: applications in future regenerative medicine. World J. Stem Cells 7, 839. https://doi.org/10.4252/wjsc.v7.i5.839.

Qi, X., Wang, H., Zhang, Y., Pang, L., Xiao, W., Jia, W., Zhao, S., Wang, D., Huang, W., Wang, Q., 2018. Mesoporous bioactive glass-coated 3D printed borosilicate bioactive glass scaffolds for improving repair of bone defects. Int. J. Biol. Sci. 14, 471–484. https://doi.org/10.7150/ijbs.23872.

Roseti, L., Parisi, V., Petretta, M., Cavallo, C., Desando, G., Bartolotti, I., Grigolo, B., 2017. Scaffolds for bone tissue engineering: state of the art and new perspectives. Mater. Sci. Eng. C 78, 1246–1262. https://doi.org/10.1016/j.msec.2017.05.017.

Ruijtenberg, S., van den Heuvel, S., 2016. Coordinating cell proliferation and differentiation: antagonism between cell cycle regulators and cell type-specific gene expression. Cell Cycle 15, 196–212. https://doi.org/10.1080/15384101.2015.1120925.

Rutkovskiy, A., Stensløkken, K.-O., Vaage, I.J., 2016. Osteoblast differentiation at a glance. Med. Sci. Monit. Basic Res. 22, 95–106. https://doi.org/10.12659/MSMBR.901142.

Sabree, I., Gough, J.E., Derby, B., 2015. Mechanical properties of porous ceramic scaffolds: influence of internal dimensions. Ceram. Int. 41, 8425–8432. https://doi.org/10.1016/J.CERAMINT.2015.03.044.

Sanz-Herrera, J.A., Boccaccini, A.R., 2011. Modelling bioactivity and degradation of bioactive glass based tissue engineering scaffolds. Int. J. Solids Struct. 48, 257–268. https://doi.org/10.1016/j.ijsolstr.2010.09.025.

Scaffaro, R., Lopresti, F., Botta, L., Rigogliuso, S., Ghersi, G., 2016. Integration of PCL and PLA in a monolithic porous scaffold for interface tissue engineering. J. Mech. Behav. Biomed. Mater. 63, 303–313. https://doi.org/10.1016/J.JMBBM.2016.06.021.

Silver, I.A., Deas, J., Erecińska, M., 2001. Interactions of bioactive glasses with osteoblasts in vitro: effects of 45S5 Bioglass, and 58S and 77S bioactive glasses on metabolism, intracellular ion concentrations and cell viability. Biomaterials 22, 175–185.

Srinivasan, S., Jayasree, R., Chennazhi, K.P., Nair, S.V., Jayakumar, R., 2012. Biocompatible alginate/nano bioactive glass ceramic composite scaffolds for periodontal tissue regeneration. Carbohydr. Polym. 87, 274–283. https://doi.org/10.1016/J.CARBPOL.2011.07.058.

Su, P., Tian, Y., Yang, C., Ma, X., Wang, X., Pei, J., Qian, A., 2018. Mesenchymal stem cell migration during bone formation and bone diseases therapy. Int. J. Mol. Sci. 19, 2343. https://doi.org/10.3390/ijms19082343.

Tamburaci, S., Tihminlioglu, F., 2018. Biosilica incorporated 3D porous scaffolds for bone tissue engineering applications. Mater. Sci. Eng. C 91, 274–291. https://doi.org/10.1016/J.MSEC.2018.05.040.

Tanaka, S., Matsuzaka, K., Sato, D., Inoue, T., 2009. Characteristics of Newly Formed Bone during Guided Bone Regeneration: Analysis of Cbfa-1, Osteocalcin, and VEGF Expression. https://doi.org/10.1563/1548-1336(2007)33[321:CONFBD]2.0.CO;2. https://doi.org/10.1563/1548-1336(2007)33[321:CONFBD]2.0.CO;2.

Tatullo, M., Marrelli, M., Shakesheff, K.M., White, L.J., 2015. Dental pulp stem cells: function, isolation and applications in regenerative medicine. J. Tissue Eng. Regenerat. Med. 9, 1205–1216. https://doi.org/10.1002/term.1899.

Turnbull, G., Clarke, J., Picard, F., Riches, P., Jia, L., Han, F., Li, B., Shu, W., 2018. 3D bioactive composite scaffolds for bone tissue engineering. Bioact. Mater. 3, 278–314. https://doi.org/10.1016/J.BIOACTMAT.2017.10.001.

Valerio, P., Pereira, M.M., Goes, A.M., Leite, M.F., 2004. The effect of ionic products from bioactive glass dissolution on osteoblast proliferation and collagen production. Biomaterials 25, 2941–2948. https://doi.org/10.1016/J.BIOMATERIALS.2003.09.086.

Verma, K., Bains, R., Bains, V.K., Rawtiya, M., Loomba, K., Srivastava, S.C., 2014. Therapeutic potential of dental pulp stem cells in regenerative medicine: an overview. Dent. Res. J. 11, 302–308.

Wang, Y., Dai, J., Zhang, Q., Xiao, Y., Lang, M., 2010. Improved mechanical properties of hydroxyapatite/poly(ϵ-caprolactone) scaffolds by surface modification of hydroxyapatite. Appl. Surf. Sci. 256, 6107–6112. https://doi.org/10.1016/J.APSUSC.2010.03.127.

Wang, Z., Wang, Y., Ito, Y., Zhang, P., Chen, X., 2016. A comparative study on the in vivo degradation of poly(L-lactide) based composite implants for bone fracture fixation. Sci. Rep. 6 https://doi.org/10.1038/srep20770.

Williams, J.M., Adewunmi, A., Schek, R.M., Flanagan, C.L., Krebsbach, P.H., Feinberg, S. E., Hollister, S.J., Das, S., 2005. Bone tissue engineering using polycaprolactone scaffolds fabricated via selective laser sintering. Biomaterials 26, 4817–4827. https://doi.org/10.1016/J.BIOMATERIALS.2004.11.057.

Wu, J., Xue, K., Li, H., Sun, J., Liu, K., 2013. Improvement of PHBV scaffolds with bioglass for cartilage tissue engineering. PLoS One 8, e71563. https://doi.org/10.1371/journal.pone.0071563.

Xu, C., Su, P., Chen, X., Meng, Y., Yu, W., Xiang, A.P., Wang, Y., 2011. Biocompatibility and osteogenesis of biomimetic Bioglass-Collagen-Phosphatidylserine composite scaffolds for bone tissue engineering. Biomaterials 32, 1051–1058. https://doi.org/10.1016/J.BIOMATERIALS.2010.09.068.

Xynos, I.D., Edgar, A.J., Buttery, L.D., Hench, L.L., Polak, J.M., 2001. Gene-expression profiling of human osteoblasts following treatment with the ionic products of Bioglass 45S5 dissolution. J. Biomed. Mater. Res. 55, 151–157.

Yu, H., Peng, J., Xu, Y., Chang, J., Li, H., 2016. Bioglass activated skin tissue engineering constructs for wound healing. ACS Appl. Mater. Interfaces 8, 703–715. https://doi.org/10.1021/acsami.5b09853.

Zhang, H., Mao, X., Du, Z., Jiang, W., Han, X., Zhao, D., Han, D., Li, Q., 2016. Three dimensional printed macroporous polylactic acid/hydroxyapatite composite scaffolds for promoting bone formation in a critical-size rat calvarial defect model. Sci. Technol. Adv. Mater. 17, 136. https://doi.org/10.1080/14686996.2016.1145532.

Zhang, H., Mao, X., Zhao, D., Jiang, W., Du, Z., Li, Q., Jiang, C., Han, D., 2017. Three dimensional printed polylactic acid-hydroxyapatite composite scaffolds for prefabricating vascularized tissue engineered bone: an in vivo bioreactor model. Sci. Rep. 7, 15255. https://doi.org/10.1038/s41598-017-14923-7.

Zhao, J., Han, W., Chen, H., Tu, M., Huan, S., Miao, G., Zeng, R., Wu, H., Cha, Z., Zhou, C., 2012. Fabrication and in vivo osteogenesis of biomimetic poly(propylene carbonate) scaffold with nanofibrous chitosan network in macropores for bone tissue engineering. J. Mater. Sci. Mater. Med. 23, 517–525. https://doi.org/10.1007/s10856-011-4468-3.